Submitted to the
XXII International Symposium on Lepton-Photon Interactions at High Energy
June 30 - July 5 2005, Uppsala, Sweden

Abstract: 295 **Session: QCD/HS**

Dijet production in diffractive deep inelastic scattering at HERA

ZEUS Collaboration

Abstract

The production of dijets in diffractive deep inelastic scattering, $ep \rightarrow e\gamma^* p \rightarrow e'p$ jet1 jet2 X$'$, has been measured with the ZEUS detector at HERA using an integrated luminosity of $65\,\text{pb}^{-1}$. This process is sensitive to the partonic structure of the diffractive exchange between the proton and the virtual photon. The dijet cross section for such processes has been measured for virtualities of the exchanged boson, $5 < Q^2 < 100\,\text{GeV}^2$ and photon-proton centre-of-mass energies, $100 < W < 250$ GeV. The jets were identified using the inclusive $k_\perp$ algorithm in the $\gamma^* p$ frame. All jets identified in each event were required to satisfy $E^*_{T,\text{jet}} > 4\,\text{GeV}$ while the jet with highest transverse energy satisfied $E^*_{T,\text{jet}} > 5\,\text{GeV}$ as measured in the $\gamma^* p$ frame. All jets were required to be in the pseudorapidity range $-3.5 < \eta^*_{\text{jet}} < 0$ in the $\gamma^* p$ frame. The cross sections were compared to the predictions from leading-logarithm parton-shower Monte Carlo models and next-to-leading-order QCD calculations based on recent diffractive parton densities extracted from inclusive diffractive deep inelastic scattering data.

1 Introduction

In diffractive events at HERA the proton interacts with the photon emitted by the lepton via colour singlet exchange. This type of process is characterized by the presence of a large rapidity gap (LRG) between the scattered proton and the dissociated photon. QCD predicts that the cross sections for diffractive deep inelastic scattering (dDIS) can be factorised into universal diffractive parton distribution functions (dPDFs) and a process-dependent coefficient which can be calculated within perturbative QCD [1]; this is known as QCD factorisation. At HERA dPDFs have been determined using inclusive diffractive DIS data [2–4].

However, predictions based on these dPDFs made for the diffractive dijet cross sections in $p\bar{p}$ collisions at the Tevatron significantly overestimate the measurements [5]. This apparent suppression of the Tevatron cross sections can be explained by considering soft rescattering processes between the diffractive final system and the outgoing beams which can destroy the LRG [6]. According to these models the same effect should be visible at HERA for processes in which the photon first fluctuates into a hadronic system before interacting with the proton ("resolved" processes), while for processes in which the photon is point-like ("direct" processes) rescattering effects should be absent [7]. Recent results show however, that such a suppression seems to occur in both direct and resolved processes [8, 9].

One important test of QCD factorisation in diffraction is to ensure that dPDFs extracted from inclusive diffractive DIS data can be used to predict the cross sections for exclusive diffractive processes. Dijet DIS processes are suited for this task for two reasons: first because jets indicate clearly the presence of a hard scale which allows the use of perturbative QCD; the other noticeable feature is that dijets processes are sensitive to the density of gluons in the diffractive exchange (i.e. via $\gamma g \to q\bar{q}$ at HERA, as shown in Fig.1) and gluons are known to carry most of the momentum of the colourless exchange [2, 3, 10].

This paper presents measurements of the cross sections for dijet production in diffractive DIS with the ZEUS detector at HERA. The measured differential cross sections are compared with leading-order (LO) and next-to-leading order (NLO) QCD predictions using the dPDFs extracted from inclusive diffractive DIS data [2–4] in order to check if QCD factorisation holds.

2 Experimental setup and data sets

This analysis uses a data sample collected with the ZEUS detector [11] at the HERA collider during the 1999-2000 data-taking period which corresponds to an integrated luminosity of 65.2 pb^{-1}. During this period HERA collided either electrons or positrons with an energy of 27.5 GeV with protons of energy 920 GeV giving a centre-of-mass energy of $\sqrt{s} = 318$ GeV. Jet reconstruction was performed using the information from the central tracking detector (CTD) [12] and the uranium-scintillator calorimeter (CAL) [13]. Diffractive events were selected by requiring a large rapidity gap in the forward region of the calorimeter (FCAL) and in the forward plug calorimeter (FPC) which was placed inside the FCAL, close to the beam pipe, in order to increase the pseudorapidity coverage in the range $4 < \eta < 5$ [1].

3 Kinematic and data selection

Dijet processes in diffractive DIS ($ep \to e'p + X(\mathrm{jet} + \mathrm{jet} + \mathrm{X}'))$ are characterized by the simultaneous presence of a scattered positron[2], a scattered proton that escapes undetected down the beam pipe and a hadronic system X, with invariant mass M_X, which contains the dijet system produced in the hard scattering and the rest of the hadronic system X'. The process is described by the following kinematic variables:

- Q^2, the photon virtuality;
- W, the virtual photon-proton centre-of-mass energy;
- $x_{\mathbb{P}}$, the momentum fraction lost by the proton;
- β, the fraction of longitudinal momentum of the colourless exchange carried by the parton struck by the photon;
- $E^*_{T,\mathrm{jet}}$ and η^*_{jet} , the transverse energy and the pseudorapidity of the jets reconstructed in the photon-proton centre-of-mass frame ($\gamma^* p$ frame).

Two further variables were used in this analysis,

$$z_{\mathbb{P}}^{\mathrm{obs}} = \frac{Q^2 + M_{12}^2}{Q^2 + M_X^2} \qquad\qquad x_{\gamma}^{\mathrm{obs}} = \frac{\sum\limits_{dijets}(E - p_z)}{\sum\limits_{hadr}(E - p_z)}$$

where M_{12} is the invariant mass of the dijet system. The variable $z_{\mathbb{P}}^{\mathrm{obs}}$ estimates the fraction of longitudinal momentum of the colourless exchange carried by the parton entering in the hard process; at LO it is equivalent to β. The quantity $x_{\gamma}^{\mathrm{obs}}$ estimates the fraction

[1] The ZEUS coordinate system is a right-handed Cartesian system, with the Z axis pointing in the proton beam direction, referred to as the "forward direction", and the X axis pointing left towards the centre of HERA. The coordinate origin is at the nominal interaction point.

[2] In the following, for simplicity,the word positron will be used to denote both electrons and positrons.

of longitudinal momentum of the virtual photon entering in the hard subprocess; in its definition the sum in the numerator runs over the two jets with highest E_T and the sum in the denominator runs over the hadronic system X.

The scattered positron was identified using a neural network [14] while jet reconstruction was performed using energy flow objects (EFO) which combine energy clusters reconstructed in the CAL and charged tracks reconstructed in the CTD [16]. The EFOs were corrected for energy losses due to the dead material present in the detector [17]. Jet reconstruction was performed with the $k_\perp$ clustering algorithm [18] which was run over corrected EFOs after having their four-momenta boosted to the $\gamma^* p$ frame. All the kinematic variables were determined using EFOs, while Q^2 and W were evaluated with the Double Angle method [15]. DIS events with a well-reconstructed vertex were selected by identifying a positron with energy higher than 10 GeV and which lies outside the region in the rear calorimeter (RCAL) around the beam pipe. The requirement $45 < \sum(E - p_z) < 65$ GeV was also imposed, where E is the energy and p_Z the component of the momentum parallel to the Z axis of a particle and the sum runs over all the particles identified in the detector. Each event was then required to contain at least two jets; all jets were required to have $E^*_{T,\mathrm{jet}} > 4$ GeV and lie in the pseudorapidity range $-2 < \eta^{\mathrm{LAB}}_{\mathrm{jet}} < 2$ in the laboratory frame which corresponds to $-3.5 < \eta^*_{\mathrm{jet}} < 0$ in the $\gamma^* p$ frame. The jet with highest transverse energy in each event must satisfy $E^*_{T,\mathrm{jet}} > 5$ GeV. This last requirement was needed by theoretical models for the NLO QCD calculations. Diffractive events were selected by requiring the presence of a LRG in the forward region. This means that the most forward EFO with energy $E_{\mathrm{EFO}} > 400$ MeV must have a pseudorapidity below 2.8 and that the total energy deposited in the FPC must be lower than 1 GeV. After all cuts, 3711 events were selected. The background coming from events in which the outgoing proton dissociates in a low mass resonance (proton dissociation background) was estimated to be the $16 \pm 4\%$ of the total cross section [20] and was subtracted from all measured cross sections. The cross sections were measured in the following kinematic region:

- $5 < Q^2 < 100$ GeV^2;
- $100 < W < 250$ GeV;
- Two or more jets with $E^*_{T,\mathrm{jet}} > 4$ GeV and the highest E^*_T jet with $E^*_{T,\mathrm{jet1}} > 5$ GeV.
- $-3.5 < \eta^*_{\mathrm{jet}} < 0.0$;
- $x_{\mathbb{P}} < 0.03$.

4 Theoretical models

Several different models were compared to the measured cross sections. Two different Monte Carlo generators were used for the LO predictions, Satrap and Rapgap. Satrap [21] uses the saturation model to describe the diffractive process and the parton shower was based on the Colour Dipole Model [22]. The cross section was derived using the proton-dipole cross section obtained from the inclusive DIS data and it does not contain the contribution of resolved processes. Rapgap [23] can be used to calculate LO cross sections for both direct and resolved processes. The "H1 fit 2" diffractive PDFs [2] and the GRV-G-HO [24] photon PDFs were used for these cross section predictions. Rapgap was interfaced to the meps [25] parton shower model and the hadronisation model jetset [26].

Using two different sets of dPDFs, two different NLO QCD predictions were determined using the DISENT [27] program adapted for diffractive processes. The dPDFs used were the "H1 2002 fit (prel.)" [3], resulting from a recent preliminary NLO QCD fit made by the H1 collaboration, and the ZEUS-LPS fit [4] obtained from the analysis of diffractive inclusive events with the ZEUS Leading Proton Spectrometer. The renormalisation scale was chosen to be the E_T^* of the highest transverse energy jet, while the factorisation scale was set to 6.8 GeV, the average E_T^* of the highest E_T^* jet. In order to take into account the theoretical uncertainties the scales were varied by factors of 0.5 and 2.0. Uncertainties of about 20% were estimated and are shown together with the NLO predictions. The Rapgap MC is used for hadronisation corrections. QED radiative corrections are evaluated from Satrap.

5 Results

The cross section is measured as a function of Q^2, W, $\log x_{\mathbb{P}}$, $\log \beta$, M_X, $E^*_{T,\mathrm{jet}}$, η^*_{jet}, $z_{\mathbb{P}}^{\mathrm{obs}}$ and x_γ^{obs} and compared to both LO and NLO predictions at the hadron level (defined as the level of stable hadrons). All jets were considered for the $E^*_{T,\mathrm{jet}}$ and η^*_{jet} cross section measurements.

The Rapgap MC was used for detector smearing and acceptance corrections. The main sources of systematic uncertainty are the choice of the Monte Carlo, the energy scale and the estimation of the proton dissociation background. The energy scale and proton dissociaton background uncertainties are shown as a shaded band in the figures.

Since the LO predictions are not expected to describe the normalisation, the cross sections predicted by both LO MCs were normalised to data. Figs.2 and 3 show that both LO Monte Carlos describe the data well. The x_γ^{obs} cross section, however, is better described by Rapgap when both resolved and direct processes are included in the model. The

RAPGAP prediction based purely on direct processes and the SATRAP prediction which contains only direct processes do not describe the shape of the cross section as a function of x_γ^{obs} (see Fig.4).

The two sets of NLO predictions evaluated from different dPDFs are compared to the data in Figs.5 and 6. The data are reasonably well described by the NLO predictions. A more detailed comparison of the data and the NLO predictions can be seen in in Figs.7, 8 and 9 in which the ratios of data to the ZEUS-LPS NLO predictions are shown. The ratios between the cross sections obtained using the H1 2002 fit (prel.) parametrisation and that using the ZEUS-LPS fit are also shown. The overall absolute normalisation of the NLO predictions based on the ZEUS-LPS fit is lower than the NLO calculations based H1 2002 fit (prel.). The former lies closer to the data. The NLO prediction has a tendency to be higher at high Q^2 and high β. This may be attributed to the uncertainty on the diffractive PDFs used in addition to missing orders as estimated by varying the renormalisation and factorisation scales. The difference in shapes for x_γ^{obs} and η^*_{jet} may be due to the presence of resolved processes not explicitly included in the NLO calculation and the uncertainty in the hadronisation corrections. Since the agreement in shape and absolute normalisation between data and NLO predictions is good, in particular considering that the uncertainty in the dPDFs is not taken in account, it can be concluded that no factorisation breaking is observed in these comparisons.

In summary the LO SATRAP and RAPGAP predictions describe the shape of the cross sections distribution well. The cross sections are also compared to the NLO predictions based on the H1 2002 fit(prel.) and ZEUS-LPS dPDFs. The description of the data is reasonable considering the uncertainties due to the scale choice and the dPDFs. Based on the choice of dPDFs used in this analysis, no evidence of QCD factorisation breaking is observed.

Aknowledgements

We are grateful to the H1 Collaboration for allowing us the use of the H1 2002 fit (prel.).

References

[1] J.C. Collins, Phys. Rev. **D 57**, 3051 (1998);
J.C. Collins, J. Phys. **G 28**, 1069 (2002).

[2] H1 Coll., C. Adloff et al., Z. Phys. **C 76**, 613 (1997).

[3] H1 Coll., *paper 980 submitted to 31st Intl. Conf. on high Energy Physics ICHEP 2002, Amsterdam, and paper 089 submitted to the EPS 2003 Conf. Aachen* (unpublished).

[4] ZEUS Coll., S. Chekanov et al., Eur. Phys. J. **C 38**, 43 (2004).

[5] CDF Coll., T. Affolder et al., Phys. Rev. Lett. **84**, 5043 (2000).

[6] A.B. Kaidalov, V.A. Khoze, A.D. Martin and M.G. Ryskin, Eur. Phys. J. **C 21**, 521 (2001);
E. Gotsman, E. Levin and U. Maor, Phys. Lett. **B 438**, 229 (1998);
B. Cox, J. Forshaw and L. Lönnblad, hep-ph/9908464.

[7] A.B. Kaidalov, V.A. Khoze, A.D. Martin and M.G. Ryskin, Phys. Lett. **B 567**, 61 (2003).

[8] ZEUS Coll., *paper 249 submitted to 32nd Intl. Conf. on high Energy Physics ICHEP 2004, Beijing, and paper 293 submitted to the EPS 2005 Conf. Lisbon* (unpublished).

[9] H1 Coll., *paper 177 submitted to 32nd Intl. Conf. on high Energy Physics ICHEP 2004, Beijing* (unpublished).

[10] ZEUS Coll., M. Derrick et al., Phys. Lett. **B 356**, 129 (1995).

[11] ZEUS Coll., U. Holm (ed.), *The ZEUS Detector*. Status Report (unpublished), DESY (1993), available on http://www-zeus.desy.de/bluebook/bluebook.html .

[12] N. Harnew et al., Nucl. Inst. Meth. **A 279**, 290 (1989);
B. Foster et al., Nucl. Phys. Proc. Suppl. **B 32**, 181, (1993);
B. Foster et al., Nucl. Inst. Meth. **A 338**, 254 (1994).

[13] M. Derrick et al., Nucl. Inst. Meth. **A 309**, 77 (1991);
A. Andersen et al., Nucl. Inst. Meth. **A 309**, 101 (1991):
A. Caldwell et al., Nucl. Inst. Meth. **A 321**, 356 (1992);
A. Bernstein et al., Nucl. Inst. Meth. **A 336**, 23 (1993).

[14] H. Abramowicz, A. Caldwell and R. Sinkus, Nucl. Inst. Meth. **A 365**, 508 (1995);
R. Sinkus and T. Voss, Nucl. Inst. Meth. **A 391**, 360 (1997).

[15] S. Bentvelsen, J. Engelen and P. Kooijinan, *Proc. Workshop on Physics at HERA*, W. Buchmuller and G. Ingelman (ed.), Vol.1, p.23, DESY, Hamburg, Germany (1992).

[16] G.M. Briskin, *Diffractive Dissociation in ep Deep Inelastic Scattering*. Ph.D. Thesis, Tel Aviv University, 1998. (unpublished).

[17] M. Wing (on behalf of the ZEUS collaboration), in *Proceedings for "10th International Conference on Calorimetry in High Energy Physics"*, CALTECH, Pasadena, USA (2002) (hep-ex/0206036).

[18] S. Catani et al., Nucl. Phys. **B 406**, 187 (1993).

[19] T. Yamashita, *Study of Three-jet Production in ep Diffractive Deep Inelastic Scattering at HERA*. Ph.D. Thesis, University of Tokyo, 2001.

[20] ZEUS Coll., S. Chekanov et al., Nucl. Phys. **B 672**, 3 (2003).

[21] K. Golec-Biernat and W. Wusthoff, Phys. Rev. **D 60**, (1999).

[22] G. Gustafson and U. Pettersson, Nucl. Phys. **B 306**, 746 (1988).

[23] H. Jung, *The RAPGAP Monte Carlo for Deep Inelastic Scattering version 2.08/00 (2001)*. See http://www.desy.de/~jung/rapgap/.

[24] M. Glück, E. Reya and A. Vogt, Phys. Rev. **D 45**, 3986 (1992);
M. Glück, E. Reya and A. Vogt, Phys. Rev. **D 46**, 1973 (1992).

[25] G. Ingelman, A. Edin and J. Rathsman, Comp. Phys. Comm. **101**, 108 (1997).

[26] M. Bengtsson and T. Sjöstrand, Comp. Phys. Comm. **46**, 43 (1987);
T. Sjöstrand, Comp. Phys. Comm. **82**, 74 (1994).

[27] S. Catani and M.H. Seymour, Nucl. Phys. **B 485**, 291 (1997);
Erratum-ibid. **B 510** 503 (1997).

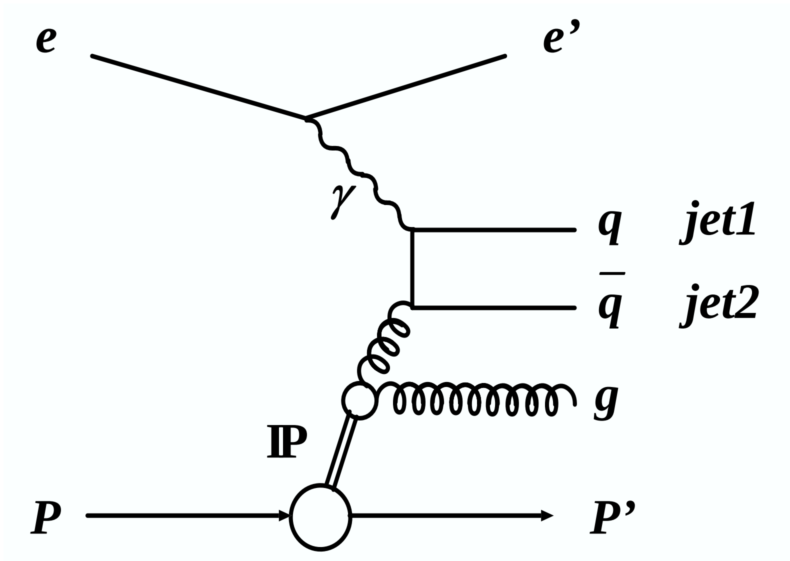

Figure 1: *The boson-gluon fusion diagram which describes at the leading-order the production of dijet in diffraction at HERA via direct photon process.*

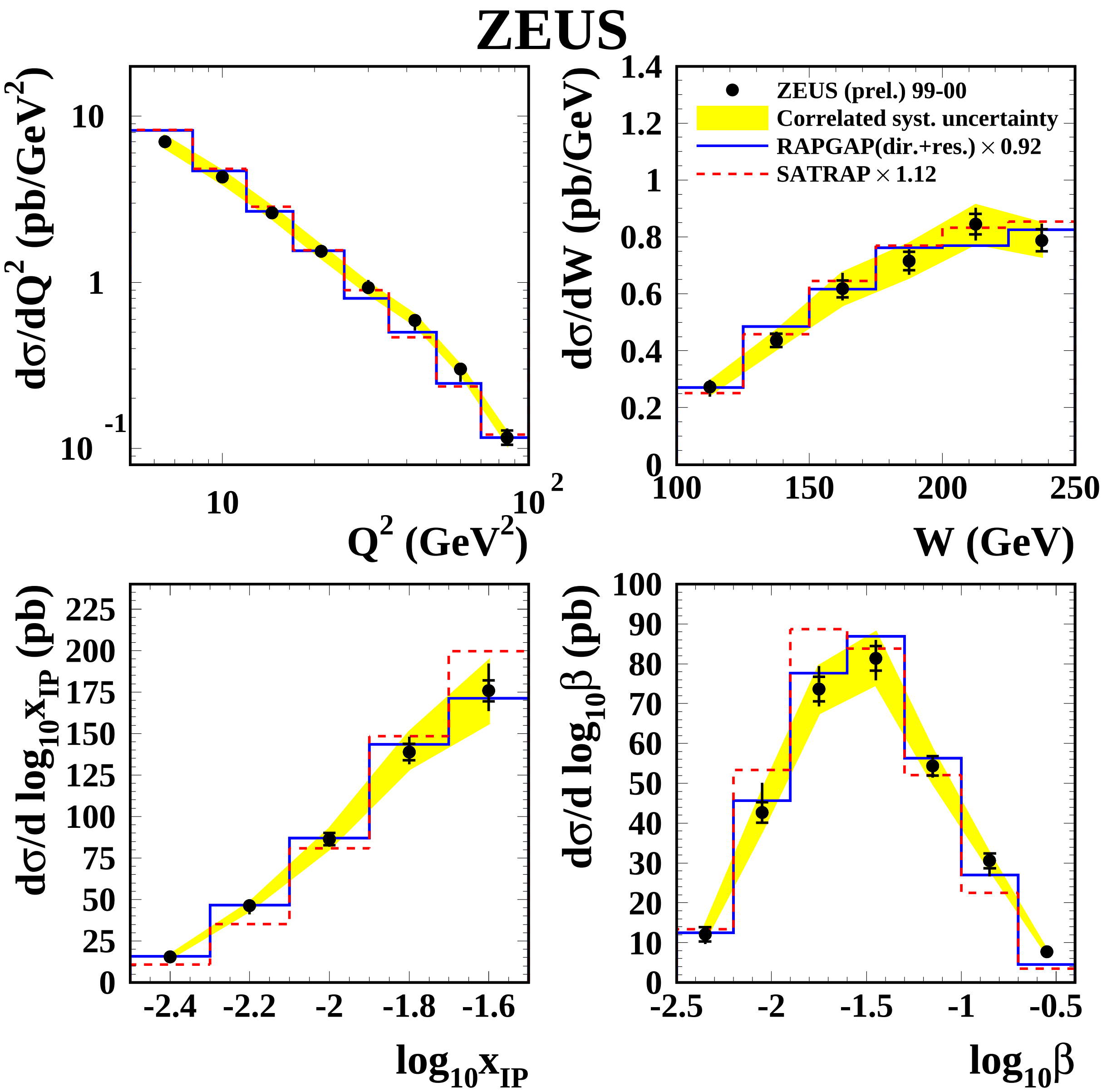

Figure 2: *The single differential cross sections as a function of Q^2, W, $log_{10}x_{\mathbb{P}}^{obs}$ and $log_{10}\beta$. The data are shown as dots; inner error bars represent the statistical uncertainty while the outer error bars represent the statistical and systematic uncertainties added in quadrature. The shaded band represents the correlated error, as described in the text. The solid lines show the prediction from the LO* RAPGAP *Monte Carlo normalised by a factor 0.92.* SATRAP *predictions normalised by a factor 1.12 are shown as dashed lines.*

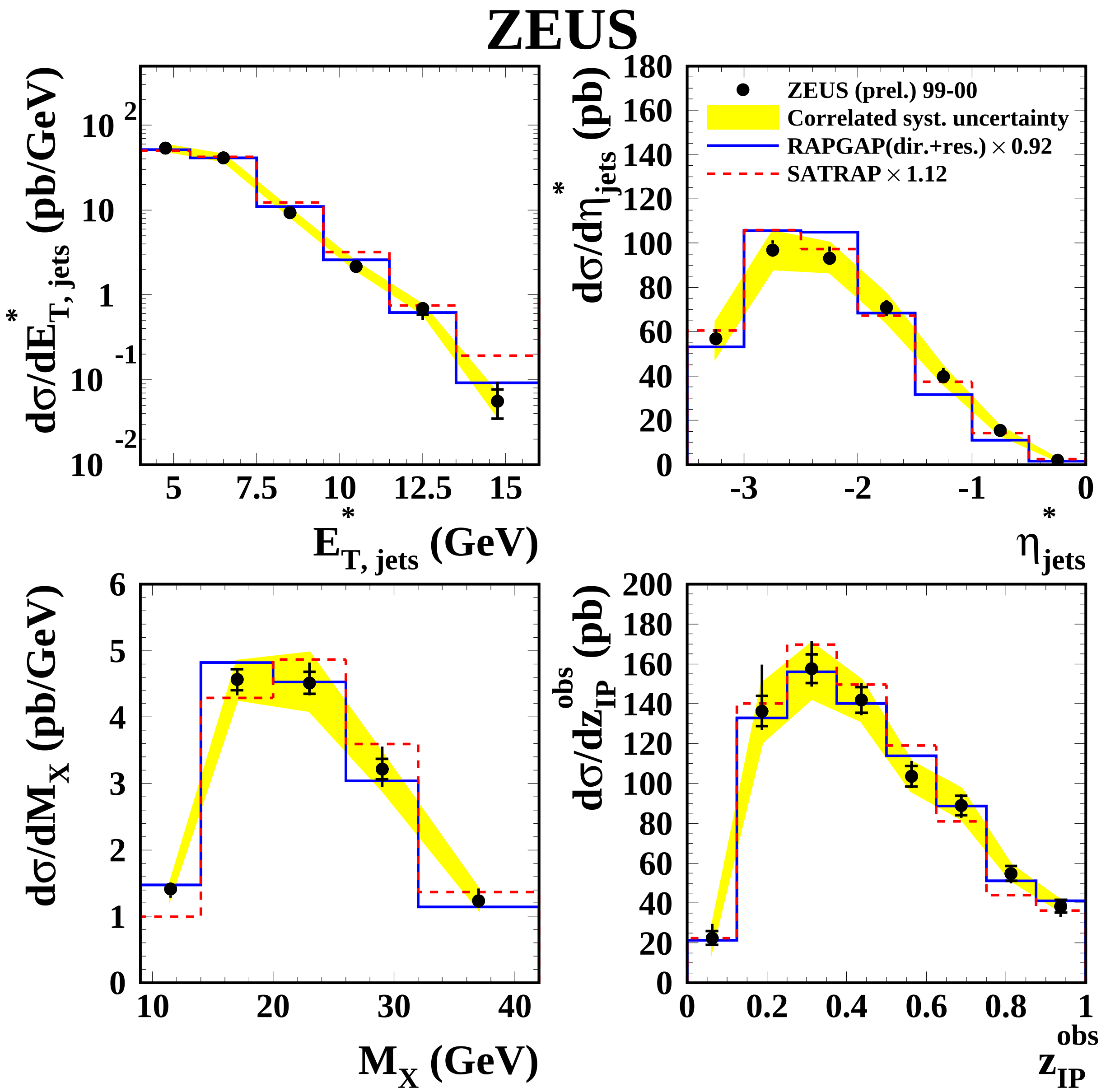

Figure 3: *The single differential cross sections in $E^*_{T,\mathrm{jet}}$, η^*_{jet}, M_X and $z_{\mathbb{P}}^{\mathrm{obs}}$. The data are shown as dots; inner error bars represent the statistical uncertainty while the outer error bars represent the statistical and systematic uncertainties added in quadrature. The shaded band represents the correlated error, as described in the text. The solid lines show the prediction from the LO* RAPGAP *Monte Carlo normalised by a factor 0.92.* SATRAP *predictions normalised by a factor 1.12 are shown as dashed lines.*

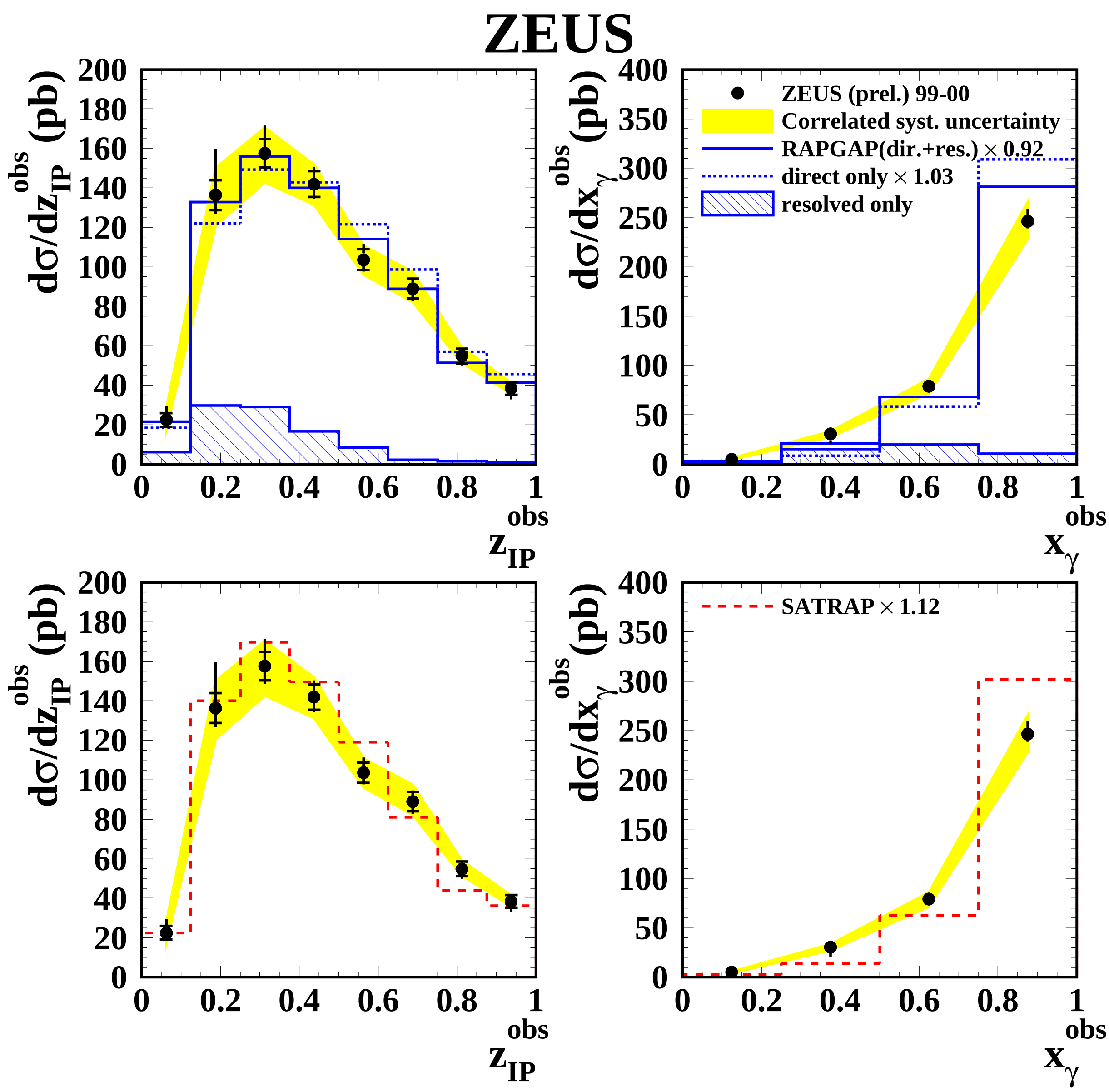

Figure 4: *The single differential cross sections in $z_{\mathbb{P}}^{obs}$ and x_γ^{obs}. The upper plots show the comparison between data (points) and* Rapgap*, both with only direct photon (dashed line) and direct plus resolved contributions (solid line). Direct only cross sections are renormalized by a factor 1.03 and direct plus resolved by a factor 0.92. The resolved component of the latter is also shown by the hatched area in order to emphatize the regions where this kind of processes is more important. The lower plots compare data (points) and the* Satrap *predictions renormalized by a factor 1.12; the* Satrap *predictions only include direct photon processes.*

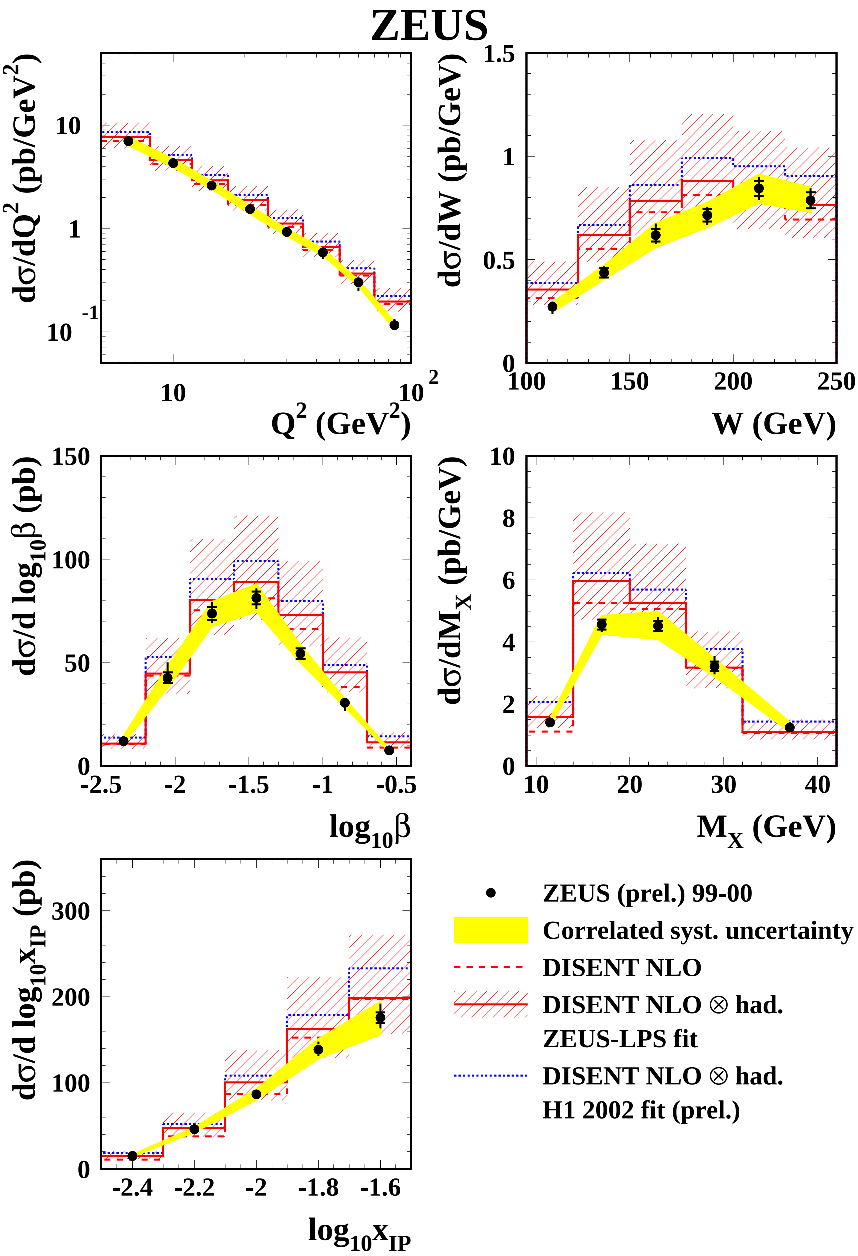

Figure 5: *The single differential cross sections in Q^2, W, $log_{10}\beta$, M_X and $log_{10}x_{\mathbb{P}}^{\rm obs}$ compared to the two NLO QCD predictions. The diffractive PDFs from the ZEUS-LPS fit and the H1 2002 fit (prel.) are used for the NLO predictions. The data are shown as dots; the inner error bars represent the statistical uncertainty while the outer error bars represent the statistical and systematic uncertainties added in quadrature. The shaded band represents the correlated error, as described in the text. Solid lines represent the NLO cross sections from the ZEUS-LPS fit; dashed lines show the same NLO predictions before hadronisation corrections. Uncertainty on these calculation due to the renormalisation scale choice is shown as a hatched area around the NLO predictions corrected for the hadronisation effects. NLO predictions from the H1 2002 fit (prel.) are drawn with a dotted line, scale uncertainties are not shown for them.*

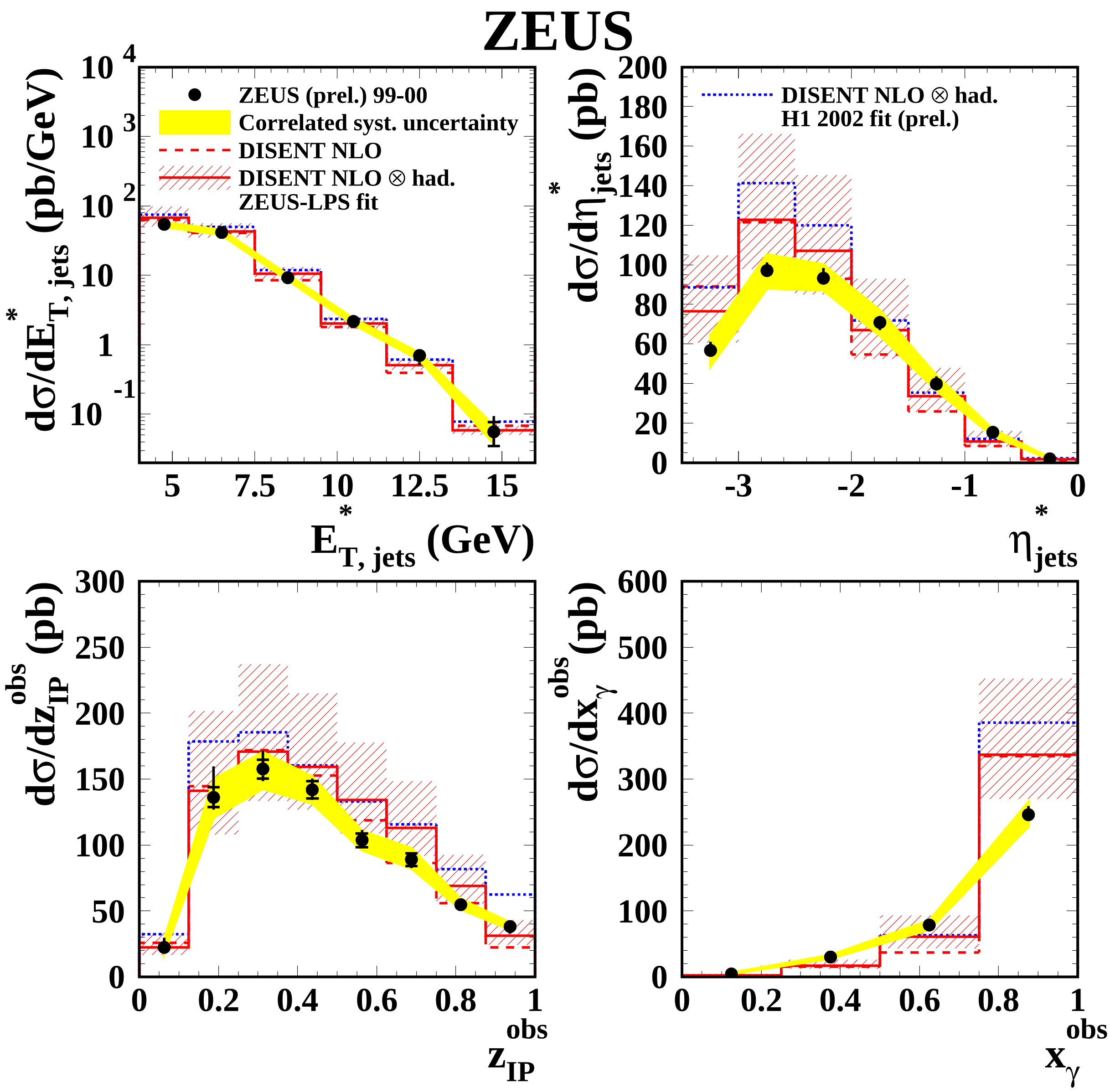

Figure 6: *The single differential cross sections in $E^*_{T,\mathrm{jet}}$, η^*_{jet}, $z^{\mathrm{obs}}_{\mathbb{P}}$ and $x^{\mathrm{obs}}_{\gamma}$ compared to the two sets of NLO QCD predictions. The data are shown as dots; inner error bars represent the statistical uncertainty while the outer error bars represent the statistical and systematic uncertainties added in quadrature. The shaded band represents the correlated error, as described in the text. Solid lines represent the NLO cross sections from the ZEUS-LPS fit; dashed lines show the NLO predictions before hadronisation corrections. Uncertainty on these calculation due to the renormalisation scale choice is shown as a hatched area around the NLO predictions corrected for the hadronisation effects. NLO predictions from the H1 2002 fit (prel.) are drawn with a dotted line, scale uncertainties are not shown for them.*

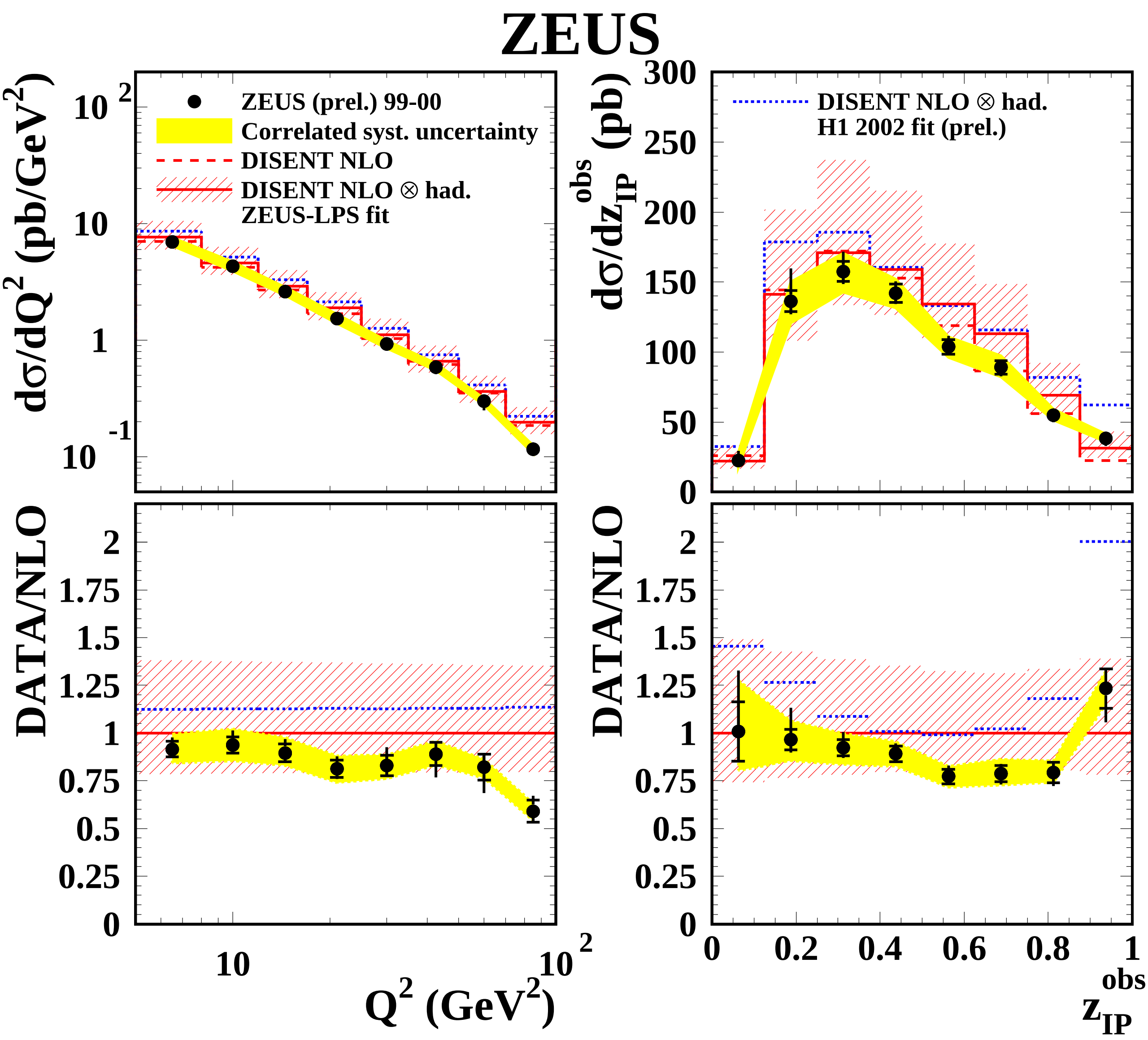

Figure 7: *Comparisons between data and NLO QCD predictions in Q^2 and $z_{\mathbb{P}}^{\rm obs}$. The upper plots show the single differential cross sections compared to the NLO QCD predictions while the lower plots show the ratio of data cross sections over NLO predictions from the ZEUS-LPS fit. The shaded band represents the correlated error, as described in the text. Solid lines with the hatched area indicate the predictions and their theoretical uncertainties. Dotted lines show the ratio of the NLO predictions from H1 2002 fit (prel.) to those from the ZEUS-LPS fit.*

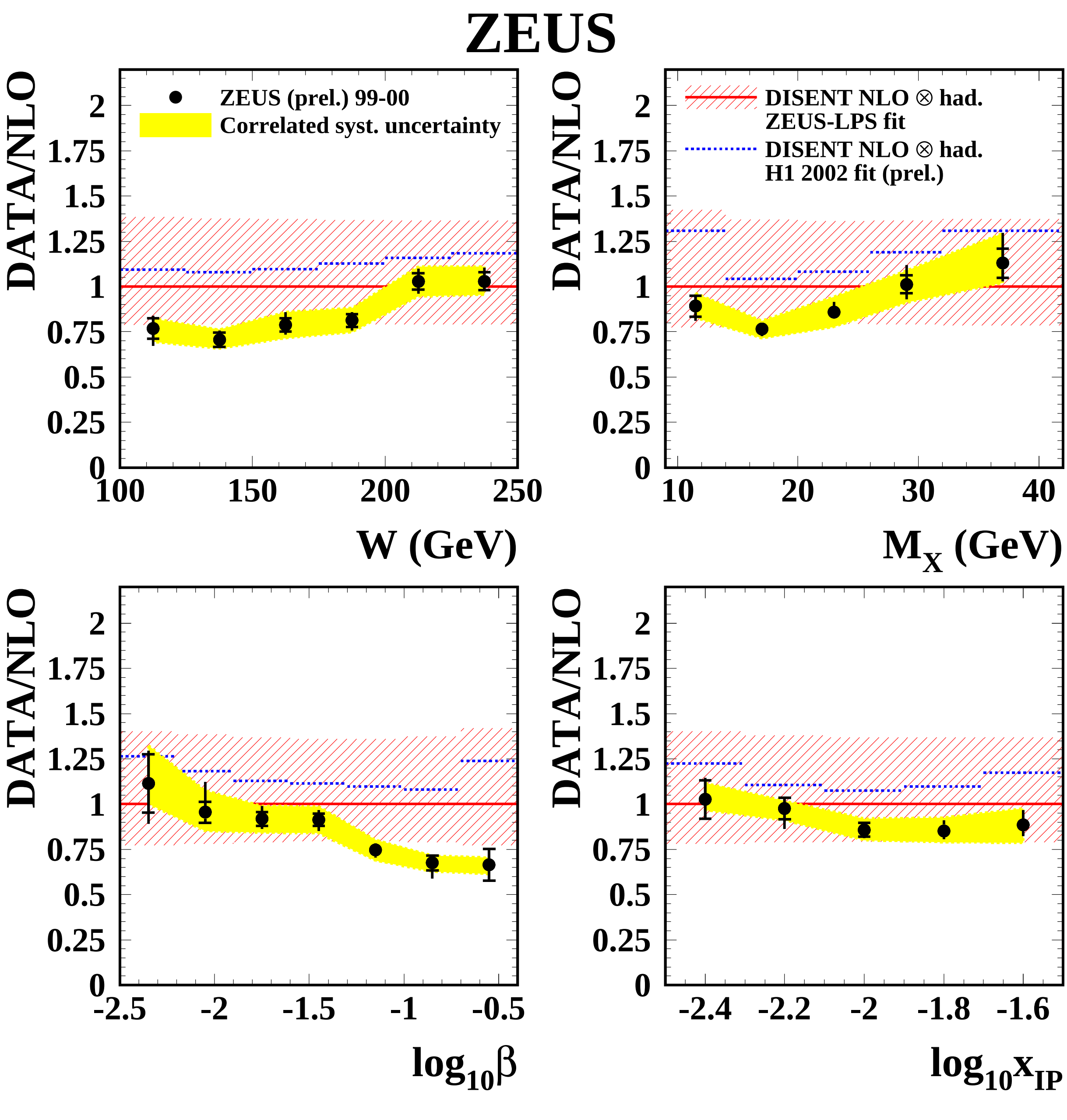

Figure 8: *Comparisons between data and NLO QCD predictions in W, M_X, log$_{10}\beta$ and log$_{10}x_{\mathbb{P}}^{\rm obs}$. The plots show the ratio of data cross sections over NLO predictions. The data are shown as dots; the inner error bars represent the statistical uncertainty while the outer error bars represent the statistical and systematic uncertainties added in quadrature. The shaded band represents the correlated error, as described in the text. Solid lines with the hatched area indicate the predictions and their theoretical uncertainties. Dotted lines show the ratio of the NLO predictions from H1 2002 fit (prel.) over the ones from ZEUS-LPS fit.*

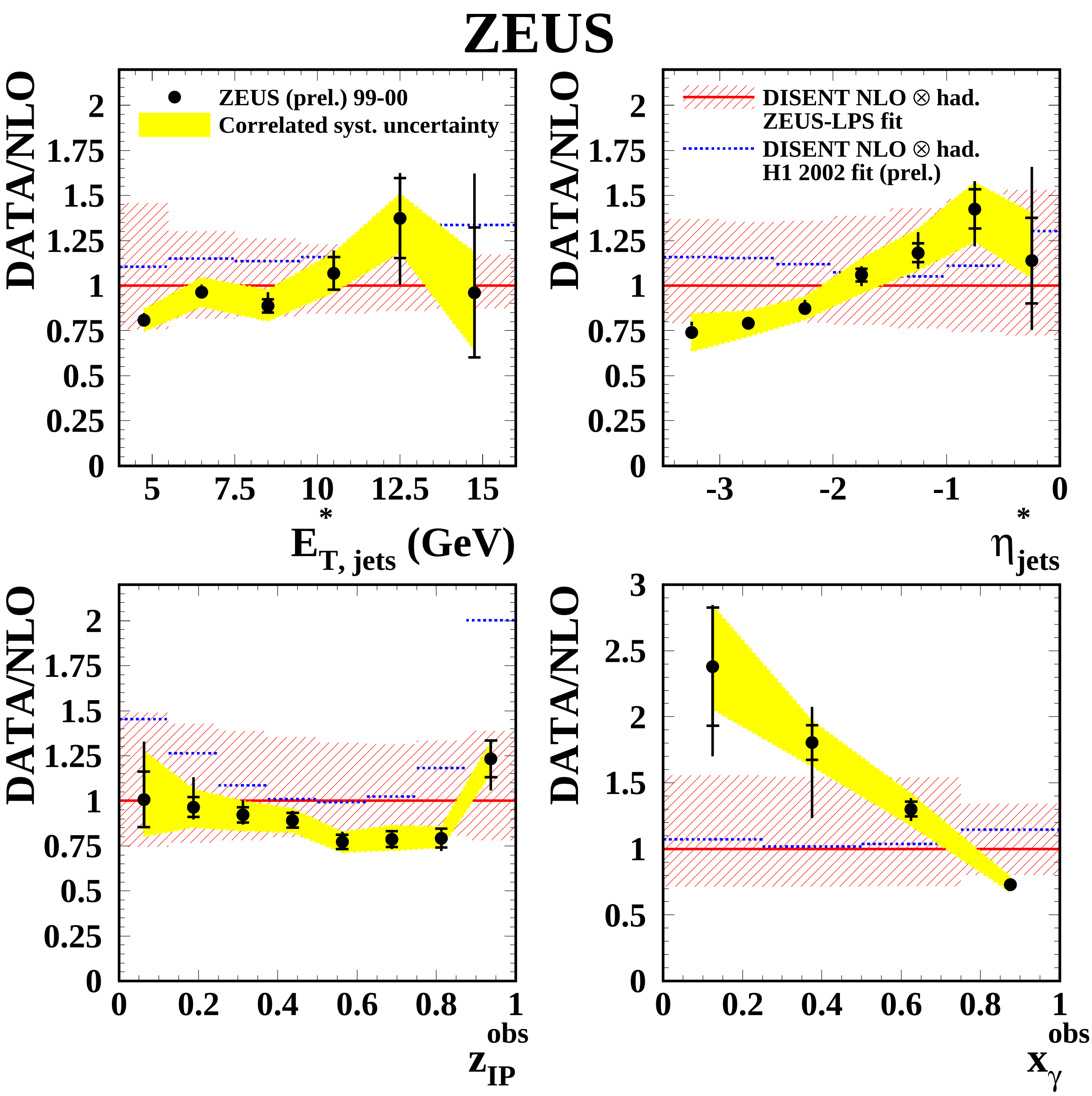

Figure 9: *Comparisons between data and NLO QCD predictions in $E^*_{T,\mathrm{jets}}$,η^*_{jets} and x_γ^{obs}. Plots show the ratio of data cross sections over NLO predictions. The data are shown as dots; inner error bars represent the statistical uncertainty while the outer error bars represent the statistical and systematic uncertainties added in quadrature. The shaded band represents the correlated error, as described in the text. Solid lines with the hatched area indicate the predictions and their theoretical uncertainties. Dotted lines show the ratio of the NLO predictions from H1 2002 fit (prel.) over those from ZEUS-LPS fit.*